

This work has been submitted to the IEEE for possible publication. Copyright may be transferred without notice, after which this version may no longer be accessible.

S^2IL : Structurally Stable Incremental Learning

S Balasubramanian, Yedu Krishna P, Talasu Sai Sriram, M Sai Subramaniam,
Manepalli Pranav Phanindra Sai, Darshan Gera
Sri Sathya Sai Institute of Higher Learning

Abstract—Feature Distillation (FD) strategies are proven to be effective in mitigating Catastrophic Forgetting (CF) seen in Class Incremental Learning (CIL). However, current FD approaches enforce strict alignment of feature magnitudes and directions across incremental steps, limiting the model’s ability to adapt to new knowledge. In this paper we propose Structurally Stable Incremental Learning (S^2IL), a FD method for CIL that mitigates CF by focusing on preserving the overall spatial patterns of features which promote flexible (plasticity) yet stable representations that preserve old knowledge (stability). We also demonstrate that our proposed method S^2IL achieves strong incremental accuracy and outperforms other FD methods on SOTA benchmark datasets CIFAR-100, ImageNet-100 and ImageNet-1K. Notably, S^2IL outperforms other methods by a significant margin in scenarios that have a large number of incremental tasks.¹

Index Terms—Class Incremental Learning, Feature Distillation, Catastrophic Forgetting, Stability, Plasticity, Structural Similarity.

I. INTRODUCTION

HUMANS continuously learn, retaining knowledge from past experiences. Efforts aim to enable machines to mimic this for solving real-world problems [1], [2]. Class Incremental Learning (CIL) [3], [4], [5], [6], [7], [8], [9], where models adapt to new classes while retaining knowledge of old ones, has gained attention. The success of deep neural networks (DNNs) has led to various approaches to CIL [10], [11], [12], [13], mainly focusing on mitigating catastrophic forgetting (CF), where adapting to new classes causes loss of previous knowledge. A key approach is feature distillation (FD), which aligns features across tasks to preserve representations of old classes while training on new ones. SOTA FD methods typically minimize the squared-norm [6], [14], or weighted squared-norm [15], [13], of the difference between feature maps from current and past tasks, with weights reflecting feature importance. However, as shown in Figure 1a and Section III-A, importance values often flatten at 1, reducing these methods [15], [13] to simple squared-norm minimization, enforcing alignment in both magnitude and direction thereby promoting stability but restricting adaptability to new classes (plasticity).

Date of submission: 20th March, 2025

All the authors are affiliated to the Department of Mathematics and Computer Science (DMACS), Sri Sathya Sai Institute of Higher Learning, Prasanthi Nilayam, India.

¹Code will be released on acceptance of the paper.

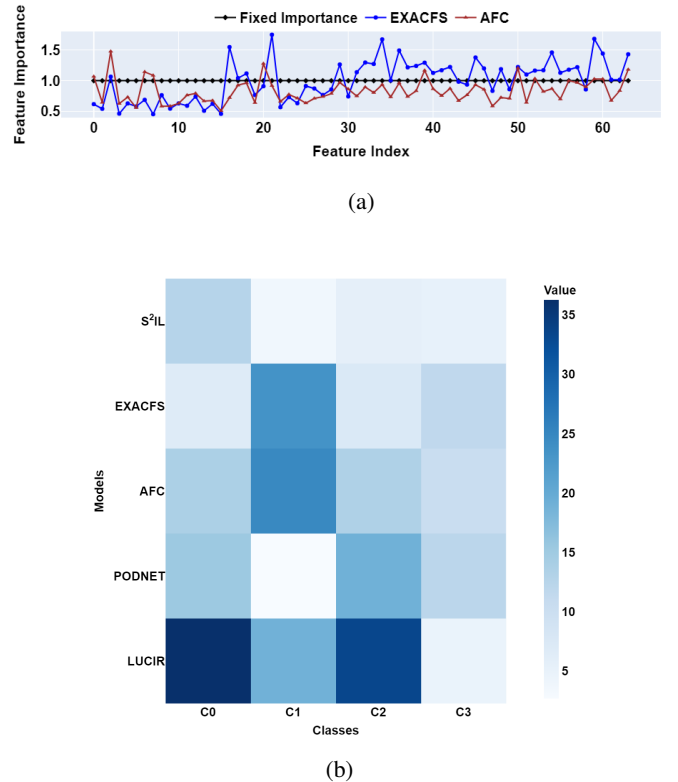


Fig. 1: A motivation for exploring structure based feature distillation (FD): (a) Average feature importance ρ across increments from the last convolutional layer of two SOTA FD models, EXACFS and AFC, evaluated on CIFAR100 with a **Inc 10** setting. Both enforce feature similarity (magnitude and direction) between increments. A feature is deemed important if it significantly influences the loss. Surprisingly, ρ remains nearly constant at 1 for all the features, for both models, limiting plasticity by enforcing feature similarity of all corresponding features equally. This highlights the need for a FD idea that balances stability with plasticity. (b) Heatmap comparing class-wise deviations in Grad-CAM feature importances of various models from those of the Oracle model O . O is trained like any other CIL model except that it has access to all past and current train data. S^2IL shows significantly lower deviation from O , suggesting that accounting for feature structure results in better generalization.

To overcome these limitations, we propose the following

contributions:

- We interpret the **Structural Similarity Index Measure (SSIM)** [16] in the CIL setting.
- A FD approach called Structurally Stable Incremental Learning (S^2IL) that preserves **structural similarity** of features across incremental steps instead of enforcing exact feature alignment, which encourages the model to retain the overall spatial patterns within features to promote flexible yet stable representations.
- The efficacy of S^2IL is demonstrated on benchmark datasets.

II. THE CIL FORMULATION

Assume $T + 1$ tasks with task 0 being the base task and the remaining tasks 1 through T arriving incrementally. The dataset for task t , $t \in \{0, 1, \dots, T\}$, is $D^t = \{(x_i^t, y_i^t)\}_{i=1}^{n^t}$ where x_i^t is the data, y_i^t is the class label and n^t is the number of samples. Each class label y_i^t belongs to C^t where $C^t = \{c_1^t, c_2^t, \dots, c_{m^t}^t\}$ represents the set of m^t classes associated with task t . For $i \neq j$, we assume $C^i \cap C^j = \emptyset$. Let $D^{0 \sim t} = \cup_{i=0}^t D^i$ and $C^{0 \sim t} = \cup_{i=0}^t C^i$. Each task t also receives a small set of exemplars E_i^t from each previously seen class c_i^t .

Depending on the context, D^t ($D^{0 \sim t}$) may refer to either the training or testing data for task t (for tasks 0 to t).

We assume a fixed convolutional network F appended with a global average pooling layer G and a growing classifier H across tasks. During training on task t , H has m^t nodes added to its existing nodes. The network F consists of L layers, with f_{ij} denoting the j^{th} feature map of layer i . Let i_{fm} represent the number of feature maps in convolutional layer i . Let $f_{(L+1)}$ denote the output of global average pooling layer G . We denote the overall model by $M = H \circ G \circ F$, where ‘ \circ ’ is the composition operation. At task t , we denote M , F , G and H by M^t , F^t , G^t and H^t , respectively. Similarly, the feature map f_{ij} at task t is denoted by f_{ij}^t . During training of M^t , the parameters of F^t and the parameters of H^t associated with the previously seen classes are initialized with parameters from the corresponding components of M^{t-1} . The new nodes of H^t are initialized using Imprinted Weights [17] as in [14]. For $t = 0$, the entire M^0 is initialized randomly.

III. THE PROPOSED S^2IL

A. Motivation

Current SOTA FD approaches [6], [14], [13], [15], in a generic sense, minimize one of the following objectives specific to feature preservation during the training of task t .

$$\sum_{i=1}^L \sum_{j=1}^{i_{fm}} \|f_{ij}^t(x) - f_{ij}^{t-1}(x)\|^2 + \|f_{L+1}^t(x) - f_{L+1}^{t-1}(x)\|^2 \quad (1)$$

$$\sum_{i=1}^L \sum_{j=1}^{i_{fm}} \rho_{ij}^t \|f_{ij}^t(x) - f_{ij}^{t-1}(x)\|^2 + \rho_{L+1}^t \|f_{L+1}^t(x) - f_{L+1}^{t-1}(x)\|^2 \quad (2)$$

where x is the input sample, $\|\cdot\|$ is Frobenius norm and ρ_{ij}^t is the importance of feature map j in layer i of F^t during training of task t , which helps preserve the learned model from

task $t - 1$. ρ_{L+1}^t is similarly defined for features from G^t . [6] considers only the second term in Eqn. (1) with normalized f_{L+1}^t , which simplifies the minimization to the maximization of $\langle f_{L+1}^t, f_{L+1}^{t-1} \rangle$, where $\langle \cdot, \cdot \rangle$ denotes the standard inner product in real space. [14] uses the term corresponding to layer $L + 1$ as is, but for the other layers, it considers the squared norm of the difference between the corresponding spatially aggregated features (aggregated separately along width and height) instead of direct comparison. [13], [15] follow the formulation in Eqn. (2), with [15] estimating the importance for each layer, feature, and class, while [13] estimating the importance only for each layer and feature.

Surprisingly, the average importance factor ρ almost flattens to 1 in both [15] and [13] across the layers. This is illustrated in Figure 1a for the last convolutional layer, which depicts the average ρ value for each feature map, averaged across all incremental tasks on the CIFAR-100 dataset where the base task consists of half the total number of classes, with 10 new classes added per incremental task. The flattening to 1 was observed in other incremental settings also, as detailed in the supplementary material. In our experiments, the difference in average incremental accuracy (AIA) between setting ρ to 1 and explicitly estimating ρ is as small as 0.4% in both [15] and [13]. In other words, both [15] and [13] effectively minimize the squared-norm of the difference between corresponding feature maps, as in Eqn. (1), with respect to feature alignment.

A key issue with minimizing terms like $\|u - v\|^2$ in Eqn. (1) is that it either aligns the direction of u and v when their sizes are constrained (e.g., normalized) or aligns both their magnitude and direction, as $\|u - v\|^2 = \|u\|^2 + \|v\|^2 - 2 \langle u, v \rangle$. Such alignment aims to make the feature representations for a given input nearly identical across tasks, preserving both the direction and magnitude of features in the feature space. However, this strict alignment can hinder the model’s plasticity by forcing it to retain exact feature representations, which reduces its capacity to adapt to new classes and patterns. While we present the reasoning for the limitation here, [8] experimentally validates the lack of plasticity in the approaches of [6], [14], and [13].

The aforementioned limitation motivated us to frame FD as a means of preserving structural similarity between features across tasks. By preserving structure, we aim to maintain the spatial arrangement of features.

This allows for more flexibility in terms of feature magnitudes and directions, providing the model room to adjust these aspects to new data, while still maintaining an overall structural similarity. This is akin to preserving the ‘shape’ rather than exact ‘positions’ in the feature space. To enforce structural similarity, we leverage SSIM [16], and refer to our proposed method as Structurally Stable Incremental Learning (S^2IL).

B. The S^2IL Loss

First, we adopt SSIM [16] for a pair of corresponding feature maps u and v between previous and current tasks respectively, and present our interpretations. SSIM between u and v is defined as:

$$\text{SSIM}(u, v) = l(u, v)^p \cdot c(u, v)^q \cdot s(u, v)^r \quad (3)$$

where

$$l(u, v) = \frac{2\mu_u\mu_v + C_1}{\mu_u^2 + \mu_v^2 + C_1} \quad c(u, v) = \frac{2\sigma_u\sigma_v + C_2}{\sigma_u^2 + \sigma_v^2 + C_2}$$

$$s(u, v) = \frac{\sigma_{uv} + C_3}{\sigma_u\sigma_v + C_3}$$

and p, q, r, C_1, C_2, C_3 are positive reals.

μ_u (μ_v) is the mean activation level of feature map u (v) across spatial dimensions. σ_u^2 (σ_v^2) quantifies the variance of feature activations around μ_u (μ_v). σ_{uv} quantifies the linear relationship between the activations of u and v , essentially capturing how well the structural patterns of u align with those of v . $l(u, v)$, the luminance component in SSIM, measures the similarity in the mean activations between the two feature maps across tasks. It reflects how well the average activations align spatially, representing their global similarity in terms of the feature values. $c(u, v)$, the contrast component, measures the similarity in the activation distributions between the two feature maps across the tasks. $s(u, v)$, the structure component, measures the similarity in the spatial relationships between the two feature maps across tasks. This captures how well the spatial patterns in u and v align, independent of their magnitudes.

l and c help maintain the global features and the distribution of features across tasks. This means that the model keeps a consistent representation of the features it has learned, even as it adapts to new tasks, without overfitting to old tasks. s ensures that as the model learns new tasks, the spatial structure of the features it learned from previous tasks is retained. This allows the model to reorganize and adjust its internal representations to incorporate new classes or tasks, without completely distorting the learned patterns from old tasks.

Given this adoption of SSIM to CIL setting, we define the FD loss during training of task t as:

$$\mathcal{L}_{S^2IL}^t = \frac{1}{|B|} \sum_{x \in B} \sum_{j=1}^{L_{fm}} \frac{1 - \text{SSIM}(f_{Lj}^t(x), f_{Lj}^{t-1}(x))}{2} \quad (4)$$

where B is the mini-batch and the inner term measures the dissimilarity between the feature maps. The inner term lies in the range $[0, 1]$ since SSIM lies in the range $[-1, 1]$. Unlike [14], [13], and [15], we apply FD only on the last convolutional layer as it contains rich semantic and structural information. Additionally, applying distillation across all layers could hinder the model’s plasticity, as discussed in [8] and validated by additional results presented in the supplementary material. The overall training of task t is governed by the loss:

$$\mathcal{L}^t = \mathcal{L}_{cls}^t + \lambda \mathcal{L}_{S^2IL}^t \quad (5)$$

where \mathcal{L}_{cls} is the local similarity classifier loss adopted from [14] and λ is a hyperparameter adopted from [13], [6] that measures the degree of need to preserve old knowledge, increasing as the ratio of new to old classes grows. The training algorithm is listed in the supplementary material.

As an empirical proof of concept for the efficacy of S^2IL , we conducted the following experiment. We defined an Oracle model O , which is incrementally trained like M , except that during task t , O has access to the entire training data of all

previous tasks, rather than just exemplars, and does not use any distillation loss. We define the deviation measure of M from O for each class $l \in C^0$ as follows:

$$D_l(M, O) = \frac{1}{L_{fm}} \sum_{j=1}^{L_{fm}} \left(1 - \frac{\alpha_{Lj,l}^{M^t} - \alpha_{Lj,l}^{O^0}}{\alpha_{Lj,l}^{O^t} - \alpha_{Lj,l}^{O^0}} \right)^2 \quad (6)$$

where $\alpha_{Lj,l}^{M^t}$ ($\alpha_{Lj,l}^{O^t}$) is the mean Grad-CAM importance [18] of the j^{th} feature map from the last convolutional layer of model $M(O)$ at task t , with the mean computed over the samples from class $l \in C^0$. This captures the influence of the j^{th} feature map on the prediction of class l . Note that Grad-CAM importance is computed post-training. The fractional term in Eqn. (6) measures the evolution of the j^{th} feature map of M relative to O across all the tasks. If M behaves similarly to O , the fractional term will be close to 1, resulting in a deviation score near 0, indicating that M maintains stability and plasticity like O . The heatmap in Figure 1b shows the deviations of S^2IL and other models including LUCIR [6], PODNet [14], AFC [13] and EXACFS [15], for a sample of base classes from CIFAR-100 under the same incremental setting as in Figure 1a. Clearly, S^2IL exhibits the lowest deviations, demonstrating its superior stability and plasticity. Additional visual plots corresponding to other base classes are provided in the supplementary material.

IV. RESULTS & DISCUSSIONS

A. Experimental Settings

The SOTA benchmark datasets used to assess the performance of the proposed S^2IL method are CIFAR-100 [19], ImageNet-1K [20] and a subset version of ImageNet-1K named ImageNet-100 [5] which has 100 randomly selected classes

from Imagenet-1K. We provide the details of these datasets in the supplementary material. Image preprocessing and class order settings follow the methodology outlined in [14]. We use ResNet-32 [14] for CIFAR-100 and ResNet-18 [14] for both ImageNet-100 and ImageNet-1K. For training, the base task (Task 0) uses half the number of total classes with the subsequent tasks taking increments of 1, 2, 5, or 10 new classes for CIFAR-100 and ImageNet-100, and 50 or 100 new classes for ImageNet-1K.

The exemplar memory budget is fixed at 2000 for CIFAR-100 and ImageNet-100, and at 20000 for ImageNet-1K, with exemplar selection based on the herding technique [5]. p, q and r for SSIM are set at 0.1, 8 and 8. Further details on hyperparameters are provided in the supplementary material. The performance metrics used in this study are AIA [5], Backward Transfer (BT) [10] and Forgetting metric (Fgt). For comparative analysis, we consider memory replay, knowledge distillation, and network expansion methods, evaluated under identical conditions.

B. Comparing S^2IL with SOTA methods

Table I shows the results. In CIFAR-100, S^2IL outperforms others, especially in the challenging **Inc 1** and **Inc 2** settings, by around 1.5%. S^2IL also performs best in the difficult **Inc 1** and **Inc 2** settings of ImageNet-100. While other

Methods	CIFAR-100				ImageNet-100			
	Inc 1	Inc 2	Inc 5	Inc 10	Inc 1	Inc 2	Inc 5	Inc 10
iCARL [5] (2017)	44.20±0.98	50.60±1.06	53.78±1.16	58.08±0.59	54.97	54.56	60.90	65.56
LUCIR [6] (2019)	49.30±0.32	57.57±0.23	61.22±0.69	64.01±0.91	57.25	62.94	70.71	71.04
BiC [21](2019)	47.09±1.48	48.96±1.03	53.21±1.01	56.86±0.46	46.49	59.65	65.14	68.97
PODNet [14] (2020)	57.86±0.38	60.51±0.62	62.78±0.78	64.62±0.65	62.48	68.31	74.33	75.54
PODNet + AANet [7] (2021)	-	62.31±1.02	64.31±0.90	66.31±0.87	-	71.78	75.58	76.96
AFC [13] (2022)	61.39±0.86	63.85±0.3	64.53±0.56	65.89±0.85	72.08	73.34	75.75	76.87
EXACFS [15] (2024)	61.1±0.75	62.75±0.8	64.05±1.05	65.48±1.08	72.5	73.78	74.96	75.93
eTag [22] (2024)	-	61.63±0.79	65.50	67.99	-	71.77	75.17	76.79
MTD [11] (2024)	60.0±1.20	62.46±0.21	65.39±0.81	66.96±0.56	70.8	73.73	76.26	77.82
S^2IL (Ours)	62.94±1.36	64.23±1.24	65.88±0.8	67.35±1.15	73.15	74.27	75.63	76.52

TABLE I: Performance Comparison using AIA (%) on CIFAR-100 and ImageNet-100. CIFAR-100 results are averaged over 3 runs. EXACFS is implemented by us. AANet, eTag, and MTD results are from [7], [22], and [11], respectively. Results for other methods are based on code from [14] and [13].

Methods	Inc 20	Inc 50	Inc 100
AFC [13] (2022)	-	67.02	68.9
MTD [11] (2024)	64.11	68.15	70.4
S^2IL (Ours)	64.84	67.23	68.9

TABLE II: Performance Comparison using AIA (%) for AFC, MTD, and S2IL on ImageNet-1K.

	iCARL	LUCIR	BiC	PODNet	AFC	EXACFS	MTD	S^2IL
BT (%)	-24.14	-11.25	-6.73	-7.98	-9.0	-9.02	-6.46	-5.3
Fgt (%)	17.5	9.1	30.9	11.9	7.5	9.01	10.9	7.3

TABLE III: Backward transfer (higher is better) and Forgetting metric (lower is better) values on the CIFAR-100 dataset with **Inc 10** setting.

distillation strategies in difficult settings like **Inc 1** prioritize stability by aligning features in magnitude and direction, they sacrifice plasticity. In contrast, S^2IL maintains both stability and plasticity, excelling in such settings. The AIA of S^2IL on ImageNet-1K is presented in the Table II, in which we notice that S^2IL performs better in the difficult INC 20 setting while MTD is does well in INC 50 and 100. Results for other methods on ImageNet-1K are presented in supplementary material. The reason for S^2IL 's better AIA in low increment settings and MTD's better AIA in large increment settings can be attributed to the multiple teachers in MTD that are forced to be diverse in their correct classifications, which is feasible with many classes per increment, boosting performance in large increment settings. However, with low increment settings, the room for diversity among teachers drops significantly. With no further FD in MTD, it forgets more unlike S^2IL . This is further highlighted by better BT and Fgt percentages for S^2IL in comparison to MTD and other methods as presented in Table III.

Param	0.1	0.2	0.4	4	8	16
p=0, q=0, r	60.22	62.01	64.08	67.17	67.18	56.7
p=0, q, r=8	67.05	67.18	67.31	67.23	66.98	67.05
p, q=8, r=8	66.92	66.97	66.68	53.78	53.9	53.63

TABLE IV: AIA (in %) of S^2IL for different values of p , q and r under **Inc 10** setting in CIFAR-100

C. Ablation Studies

We performed an ablation study on the SSIM parameters p , q , and r over the set of values $\{0.1, 0.2, 0.4, 4, 8, 16\}$ under

Our Model with	AIA (%)
only l	60.82±0.65
only c	62.52±1.02
only s	67.65±0.97
$l+c$	64.76±0.74
$l+s$	67.18±1.18
$c+s$	67.59±1.17
$l+c+s$	67.35±1.15

TABLE V: Ablation study on components of SSIM (**Inc 10**, CIFAR-100, mean over 3 runs)

the CIFAR-100 **Inc 10** setting. First, we optimized r for the structure component, then q with r fixed, and finally p with both r and q fixed. Results are shown in Table IV. While $q = 0.4$ and $q = 4$ slightly outperforms $q = 8$ on CIFAR-100, we selected $q = 8$ as it yielded marginally better results on ImageNet-100. Additionally, we investigated the impact of the SSIM components l , c , and s on the model performance. As shown in Table V, the absence of the structure component leads to a sharp performance drop, highlighting its importance. Despite a marginal improvement from using only structure in CIFAR-100 **Inc 10** setting, incorporating all three components (l , c , and s) provided better results on ImageNet-100, guiding our final choice (refer to the supplementary material). More ablation studies are presented in the supplementary material.

V. CONCLUSIONS

FD methods in the literature force equality in the direction and magnitude among feature maps which impair the model's plasticity. The proposed method, S^2IL , effectively balances the stability-plasticity dilemma by enforcing structural similarity between feature maps across incremental tasks through the incorporation of SSIM. We also validated our method by testing it on SOTA benchmark datasets over the AIA, BT and Fgt metrics and find that S^2IL delivers strong and comparable performance without enforcing direct feature preservation across tasks.

Computing SSIM requires either the forward propagation of exemplars through a stored copy of the old model, or retaining feature maps of all exemplars, leading to an additional memory overhead. This can pose challenges for implementation in memory-constrained settings. Recent works in CIL focus on exemplar-free approaches and it would be interesting to

incorporate S^2IL in such scenarios where the need for storing exemplars is eliminated.

REFERENCES

- [1] R. Gupta, A. Roy, C. Christensen, S. Kim, S. Gerard, M. Cincebeaux, A. Divakaran, T. Grindal, and M. Shah, "Class prototypes based contrastive learning for classifying multi-label and fine-grained educational videos," in *CVPR*, June 2023, pp. 19 923–19 933.
- [2] J. Park, M. Kang, and B. Han, "Class-incremental learning for action recognition in videos," in *ICCV*, October 2021, pp. 13 698–13 707.
- [3] I. Kuzborskij, F. Orabona, and B. Caputo, "From n to n+1: Multiclass transfer incremental learning," in *CVPR*, June 2013.
- [4] Z. Li and D. Hoiem, "Learning without forgetting," in *ECCV*, 2016.
- [5] S.-A. Rebuffi, A. Kolesnikov, G. Sperl, and C. H. Lampert, "icarl: Incremental classifier and representation learning," in *CVPR*, July 2017.
- [6] S. Hou, X. Pan, C. C. Loy, Z. Wang, and D. Lin, "Learning a unified classifier incrementally via rebalancing," in *CVPR*, June 2019.
- [7] Y. Liu, B. Schiele, and Q. Sun, "Adaptive aggregation networks for class-incremental learning," in *CVPR*, June 2021, pp. 2544–2553.
- [8] D. Kim and B. Han, "On the stability-plasticity dilemma of class-incremental learning," in *CVPR*, June 2023, pp. 20 196–20 204.
- [9] J. He, "Gradient reweighting: Towards imbalanced class-incremental learning," in *CVPR*, June 2024, pp. 16 668–16 677.
- [10] S. Yan, J. Xie, and X. He, "Der: Dynamically expandable representation for class incremental learning," in *CVPR*, June 2021, pp. 3014–3023.
- [11] H. Wen, L. Pan, Y. Dai, H. Qiu, L. Wang, Q. Wu, and H. Li, "Class incremental learning with multi-teacher distillation," in *CVPR*, June 2024, pp. 28 443–28 452.
- [12] F. Zenke, B. Poole, and S. Ganguli, "Continual learning through synaptic intelligence," in *ICML*, 2017.
- [13] M. Kang, J. Park, and B. Han, "Class-incremental learning by knowledge distillation with adaptive feature consolidation," in *CVPR*, June 2022, pp. 16 071–16 080.
- [14] A. Douillard, M. Cord, C. Ollion, T. Robert, and E. Valle, "Podnet: Pooled outputs distillation for small-tasks incremental learning," in *ECCV*, 2020.
- [15] S. Balasubramanian, M. S. Subramanian, T. S. Sriram, S. M. P. Phanindra, P. Yedu Krishna, D. Gera, and R. Mukkamala, "Exacfs - a cil method to mitigate catastrophic forgetting," in *Proceedings of the Fifteenth Indian Conference on Computer Vision Graphics and Image Processing*, ser. ICVGIP '24. New York, NY, USA: Association for Computing Machinery, 2025. [Online]. Available: <https://doi.org/10.1145/3702250.3702267>
- [16] Z. Wang, A. Bovik, H. Sheikh, and E. Simoncelli, "Image quality assessment: from error visibility to structural similarity," *IEEE TIP*, vol. 13, no. 4, 2004.
- [17] H. Qi, M. Brown, and D. G. Lowe, "Low-shot learning with imprinted weights," in *CVPR*, June 2018.
- [18] R. R. Selvaraju, M. Cogswell, A. Das, R. Vedantam, D. Parikh, and D. Batra, "Grad-cam: Visual explanations from deep networks via gradient-based localization," in *ICCV*, Oct 2017.
- [19] A. Krizhevsky and G. Hinton, "Learning multiple layers of features from tiny images," 2009, cIFAR-100 dataset. [Online]. Available: <https://www.cs.toronto.edu/~kriz/cifar.html>
- [20] J. Deng, W. Dong, R. Socher, L.-J. Li, K. Li, and L. Fei-Fei, "Imagenet: A large-scale hierarchical image database," in *CVPR*. Ieee, 2009, pp. 248–255.
- [21] Y. Wu, Y. Chen, L. Wang, and Y. Ye, "Large scale incremental learning," in *CVPR*, 2019, pp. 374–82.
- [22] L. Huang, Y. Zeng, C. Yang, Z. An, B. Diao, and Y. Xu, "etag: Class-incremental learning via embedding distillation and task-oriented generation," *AAAI*, vol. 32, no. 11, pp. 12 591–12 599, 2024.

APPENDIX

Algorithm 1 Training at Task t

-
- 1: **Input:**
 - 2: D^t : Training data for task t
 - 3: $E^{0 \sim t-1}$: Set of exemplars from tasks $\{0, \dots, t-1\}$
 - 4: p, q, r : SSIM params set to 0.1, 8, and 8, respectively
 - 5: M^{t-1} : Trained model from task $t-1$
 - 6: λ : Weight for S^2IL loss \mathcal{L}_{S^2IL}
 - 7: **Output:** Trained model M^t
 - 8: **Initialization:** $F^t \leftarrow F^{t-1}$
 - 9: For $(x, y) \in D^t \cup E^{0 \sim t-1}$
 - 10: Compute $\mathcal{L}_{S^2IL}(x)$ and $\mathcal{L}_{cls}(x)$
 - 11: $\mathcal{L}(x) = \mathcal{L}_{cls}(x) + \lambda \mathcal{L}_{S^2IL}(x)$
 - 12: Backpropagate and update model parameters
-

We utilized the following benchmark datasets: CIFAR-100, ImageNet100, and ImageNet-1K. The CIFAR-100 dataset [19] contains 60,000 color images across 100 classes, each with a resolution of 32×32 . It is divided into 50,000 training images and 10,000 test images. ImageNet100 [5] is a subset of the original ImageNet-1K [20], consisting of 100 randomly selected classes, each containing approximately 1,300 color images. The sampling method for ImageNet100 is detailed in [6], [14]. ImageNet-1K comprises over 1.2 million labelled training images across 1,000 object categories, with an additional 50,000 validation images. It serves as a key benchmark for evaluating machine learning models in image classification tasks.

A. AFC[8] and EXACFS[15] Importance Values Flatten to 1

We present visuals in Figure 2 for other incremental settings than the one considered in Figure 1a in the manuscript to show that importances estimated by AFC and EXACFS flatten to 1. Specifically, only 10%, 4%, and 1% of the feature importances are significant for AFC in the **Inc 1**, **Inc 2**, and **Inc 10** settings, respectively. For EXACFS, only 1% of the feature importances appear significant in all cases.

B. Deviations from Oracle Model

We present here in Figure 3 the deviations in Grad-CAM feature map importance values of various models compared to the Oracle model on the CIFAR-100 dataset for all the 50 base classes. Unlike the heatmap in Figure 1b (that presented deviations for a sample of classes only), which would become too large and cluttered due to all the 50 classes considered here, we use a boxplot to display these deviations, summarizing the statistics across all classes. The results clearly show that S^2IL exhibits the smallest deviation from the Oracle model.

The model is trained on CIFAR-100, ImageNet-100, and ImageNet-1K datasets using SGD with a momentum of 0.9. For CIFAR-100, training is conducted over 160 epochs with a batch size of 128, a weight decay of 0.0005, and an initial learning rate of 0.1, which is decayed using a *CosineAnnealingScheduler*. For ImageNet-100 and ImageNet-1K, training spans 90 epochs with a batch size of 64, a weight decay of 0.0001, and an initial learning rate of 0.05, also decayed via

the *CosineAnnealingScheduler*. The loss function employed is the local similarity classifier loss [14], featuring a margin of 0.6, a learnable scale factor initialized to 1.0, and 10 proxies per class. The regularization coefficient (λ) in Equation (5) is configured as $4 \times \sqrt{(|C^{0 \sim t}|/|C^t|)}$ for CIFAR-100 and $10 \times \sqrt{(|C^{0 \sim t}|/|C^t|)}$ for ImageNet datasets. Following initial training, the model undergoes fine-tuning for 20 epochs on a balanced dataset encompassing samples from all seen classes, with learning rates of 0.05 for CIFAR-100 and 0.02 for both ImageNet-100 and ImageNet-1K.

Here we present the results for all the models considered for the comparative analysis of S^2IL , in Table VI for the incremental settings of Inc 50 and Inc 100

Methods	ImageNet-1K	
	Inc 50	Inc 100
iCARL [5] (2017)	46.72	51.36
LUCIR [6] (2019)	61.28	64.34
BiC [21](2019)	44.31	45.72
PODNet [14] (2020)	64.13	66.95
PODNet + AANet [7] (2021)	64.85	67.73
AFC [13] (2022)	67.02	68.9
EXACFS [15] (2024)	-	-
eTag [22] (2024)	-	-
MTD [11] (2024)	68.15	70.4
S^2IL (Ours)	67.23	68.9

TABLE VI: Performance Comparison using AIA (%) on ImageNet-1K. EXACFS and eTag results are not available for ImageNet-1K. MTD results are from [11].

C. Distillation across All layers vs Last layer

The Average Incremental Accuracy of S^2IL , when applied on all convolution layers and when applied on last convolution layer is presented in Table VII for CIFAR-100 dataset. The significant performance gap demonstrates that applying distillation across all layers may impair the model’s plasticity.

Incremental Setting	All Layers	Last Layer
Inc 1	57.69	62.93
Inc 2	59.72	64.04
Inc 5	63.02	65.56
Inc 10	65.05	66.74

TABLE VII: Average Incremental Accuracy (%) of S^2IL applied to all layers vs. last layer

D. Impact of SSIM components on S^2IL

As discussed in the Ablation Studies section of the manuscript, incorporating all the three components of SSIM provides marginally better results on ImageNet-100 as shown in Table VIII. The Average Incremental Accuracy of S^2IL when using only the structure component for **Inc 1, 2, 5 & 10** on ImageNet-100 is .3% to 2.5% lower than when all components are included. This guides us to the choice of applying all three components of SSIM with the values 0.1, 8.0 and 8.0 for the exponent components p, q and r respectively in the SSIM formula.

Incremental Setting	<i>only s</i>	<i>l + c + s</i>
Inc 1	70.7	73.15
Inc 2	71.7	74.27
Inc 5	75.54	75.63
Inc 10	76.18	76.52

TABLE VIII: Average Incremental Accuracy (%) of S^2IL with only structure component on ImageNet-100

E. Memory Ablation

We explored two memory allocation strategies: (1) a fixed budget of 20 exemplars per class, denoted as M1, and (2) a fixed overall memory budget of 2000 exemplars, equally distributed across the previously seen classes during incremental training, denoted as M2. Table IX presents the results, which show a clear advantage of M2 over M1. Therefore, we adopt the M2 strategy for our model.

Type	Inc 1	Inc 2	Inc 5	Inc 10
M1 (CIFAR-100)	62.93	64.04	65.56	66.74
M1 (ImageNet-100)	72.9	74.25	75.55	76.05
M2 (CIFAR-100)	62.94	64.23	65.88	67.35
M2 (ImageNet-100)	73.15	74.27	75.63	76.52

TABLE IX: Exemplar memory type study

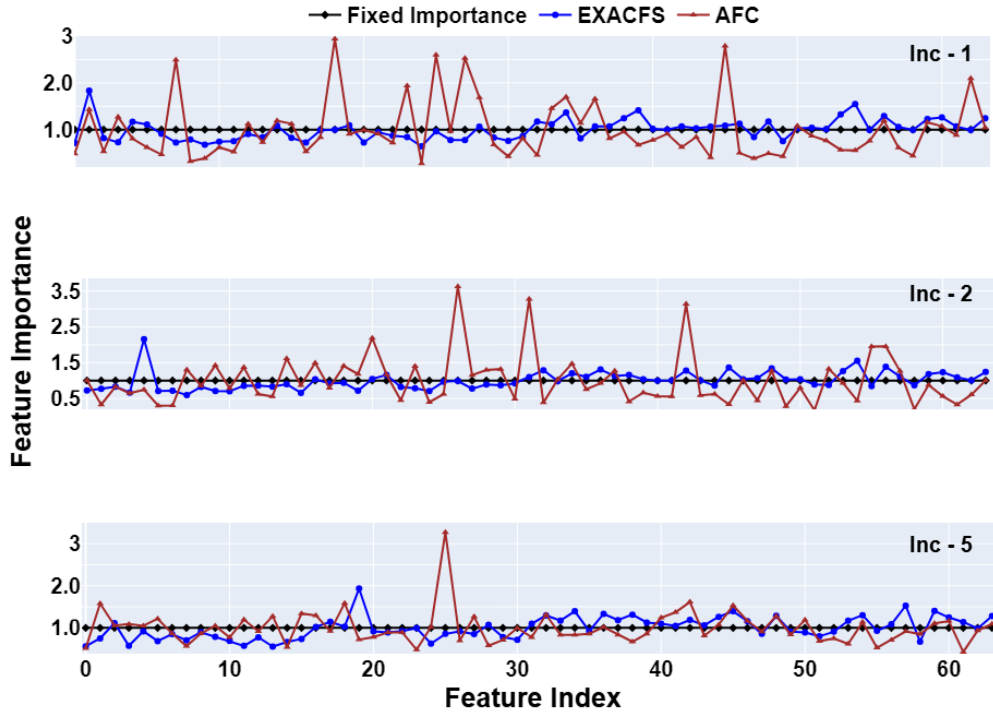


Fig. 2: Figure 1a from the manuscript extended for other incremental settings on the CIFAR-100 dataset. The importance values computed by AFC [22] and EXACFS [4] are predominantly flattened to 1.

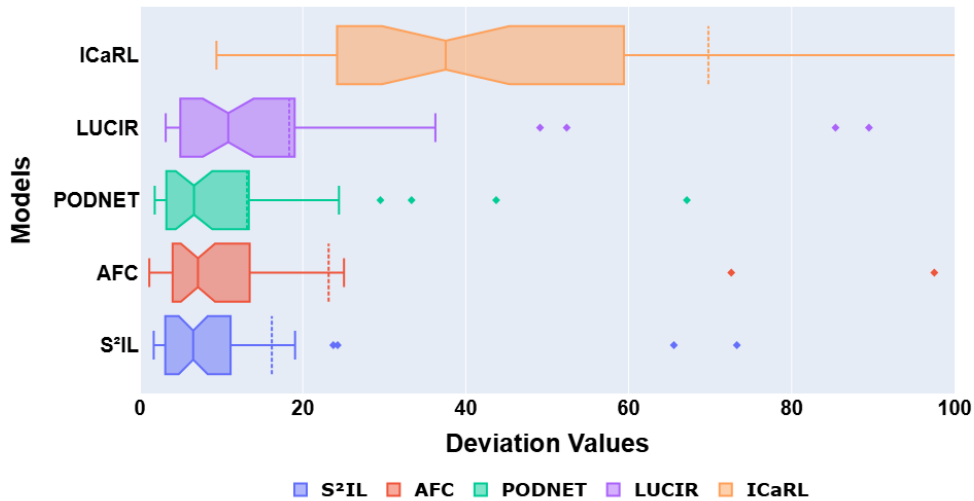


Fig. 3: Boxplot of deviations in Grad-CAM feature map importance values of various models compared to the Oracle model on the CIFAR-100 dataset